Resonant Scattering of Emission Lines in Coronal Loops: Effects on Image Morphology and Line Ratios

Kenneth Wood and John Raymond

Harvard-Smithsonian Center for Astrophysics, 60 Garden Street, Cambridge, MA 02138

kenny@claymore.harvard.edu, jraymond@cfa.harvard.edu

ABSTRACT

We have investigated the effects of resonant scattering of emission lines on the image morphology and intensity from coronal loop structures. It has previously been shown that line of sight effects in optically thin line emission can yield loop images that appear uniformly bright at one viewing angle, but show "looptop sources" at other viewing angles. For optically thick loops where multiple resonant scattering is important, we use a 3D Monte Carlo radiation transfer code. Our simulations show that the intensity variation across the image is more uniform than the optically thin simulation and, depending on viewing angle, the intensity may be lower or higher than that predicted from optically thin simulations due to scattering out of or into the line of sight.

Subject headings: line: formation — scattering — Sun: corona — Sun: X-rays — radiative transfer

1. Introduction

Two effects of resonant line scattering on emission lines are to change the morphology of images and to change line ratios from what would be expected from optically thin analyses. Qualitatively, the effects can be split into three broad optical depth categories, low, moderate, and large. At low optical depths ($\tau < 5$) resonant scattering primarily changes the photon direction and photons emerge into the directions of lowest optical depth. At moderate optical depths ($\tau \sim 10 - 100$) multiple scattering is important and there is a large probability of photon energy conversion, e.g., the conversion of Lyβ photons to Hα photons. Large optical depths ($\tau >> 100$) result in photon trapping and collisional

de-excitation, eventually leading to thermalization. The goal of this paper is to investigate the effects of resonant scattering on images and intensity ratios in the low optical depth regime. Situations where our work is applicable include UV, EUV, and soft X-ray emission line imaging and spectroscopy of the Sun and stellar coronae. While we have chosen a geometry based on coronal magnetic loops, similar considerations would apply, for instance, to some of the strong X-ray emission lines in older supernova remnants. We have simulated an X-ray line of Fe XVII, but the predicted effects on image morphology should be visible in the narrow-band EUV images of EIT and TRACE.

Ultraviolet and soft X-ray emission line ratios are frequently used as diagnostics of temperature, density, elemental abundances, and the ionization state of astrophysical plasmas. Several assumptions are often implicitly made when emission line ratios are analyzed. In particular, the optical depth is generally assumed to be negligible. However, solar coronal observations of the Fe XVII line at 15.01Å show line ratios that are lower than theoretical predictions (Phillips et al. 1997; Schmelz et al. 1997; Saba et al. 1999; Waljeski et al. 1994) or laboratory measurements (Brown et al. 1998). Rugge & MacKenzie (1985) suggested that optically thick resonant scattering of Fe XVII 15.01Å photons out of the line of sight may be responsible for the small line ratios. Saba et al. (1999) employed the escape probability method of Kastner & Kastner (1990) in their analysis of various line ratios and found that up to 50% of the Fe XVII flux is unaccounted for. Bhatia & Kastner (1999) found similar results for planar and cylindrical geometries. This explanation for the intensity decrements is likely, given the large oscillator strength of the Fe XVII 15.01Å line (Table 1). For typical densities ($n_e \sim 10^{10}$) and sizescales ($\sim 10^9$cm) in the solar corona, the optical depth of the Fe XVII 15.01Å line is around 1. This is in the low optical depth regime in which the major effect is scattering of photons into optically thin directions.

In this paper we present three dimensional Monte Carlo radiation transfer simulations of the transfer of Fe XVII 15.01Å photons. Our analysis does not treat transfer within the line itself, instead considering all photons to be emitted and resonantly scattered at a single wavelength. This approximation is valid so long as the optical depth is not large enough that photons scatter out of the Doppler core. The advantage of our Monte Carlo technique is that it naturally accounts for arbitrary illumination and multiple scattering in complex geometries. The results of our Monte Carlo simulations are images that may be compared directly with optically thin simulations to determine differences in image morphology and optically thick to optically thin intensity ratios.

Previous simulations by Alexander & Katsev (1996) produced optically thin images of loops in which the density and temperature follow the scaling law prescription of Rosner, Tucker, & Vaiana (1978, hereafter RTV). The simulations of Alexander & Katsev showed

that it is crucial to consider the geometry and temperature dependence of the emissivity along with the thermal response of the imaging telescope when analyzing solar emission line images. Such images may be in the light of a single line or an ensemble of lines as is the case with the broad wavelength response of Yohkoh SXT. In particular, a loop viewed face-on may appear uniformly bright, but line-of-sight effects can yield an apparent "looptop" source when the same loop is viewed close to edge-on (see Fig. 5 of Alexander & Katsev). Our work is a natural extension of the Alexander & Katsev analysis to optically thick, multiple scattering situations, and for continuity purposes we also adopt RTV loops for our simulations.

Section 2 presents the model ingredients (loop structure, Fe XVII emissivity and opacity, and radiation transfer technique). Results of our simulations (images and intensity ratios of optically thick/optically thin models) are presented in § 3, and in § 4 we discuss our results with respect to observational data.

2. Model Ingredients

In order to construct model images we must specify the emissivity, opacity, and scattering geometry within our Monte Carlo radiation transfer code. These model ingredients are now described.

2.1. Loop Structure

Following Alexander & Katsev, we consider loops with a density and temperature structure given by the RTV scaling law model. The RTV model is a hydrostatic loop model in which the maximum loop temperature, $T_{\max}$, and loop length, L, are related to the pressure, p, by $T_{\max} \sim 1.4 \times 10^3 (pL)^{1/3}$. The maximum temperature occurs at the loop apex, and the balance among thermal conduction, radiative cooling and mechanical heating determines the temperature distribution along the length of the loop. An RTV loop is therefore specified by two parameters, the maximum temperature, $T_{\max}$, and loop length, L, measured along the loop from a footpoint to the looptop. Throughout our simulations we assume the loops are semicircular tori with length $L = 10^{10}$ cm and radius $r = L/10$. We then construct simulations for a range of maximum temperatures and viewing angles. See Fig. 1 for a diagram showing the loop length, radius, and orientation.

In some cases we embed the emitting loop in a lower density background plasma. Alexander & Katsev modeled isolated loop structures. We wish to investigate situations

where a background plasma may provide additional scattering opacity, thereby allowing for attenuation of loop emission and the formation of scattering halos around the loops. For the background we embed the RTV loop in a hemispherical isothermal constant density plasma. We adopt a temperature of $T = 2.5 \times 10^6$K and set the density such that the total emissivity from the hemispherical volume is half of that emanating from the RTV loop (see § 3).

We note here that an isothermal, constant density background plasma may be physically unrealistic. The precise form of the background is unimportant for the purposes of this work, as we wish to show the general effects of resonant scattering. For future modeling of images from TRACE, EIT, and SXT where resonant scattering effects are important, more realistic loop structures and backgrounds will be generated.

2.2. Fe XVII Emissivity and Opacity

The Fe XVII 15.01 Å line emissivity and opacity are functions of temperature within the loop. The Fe abundance was taken as the typical FIP (first ionization potential) enhanced value of three times the photospheric abundance (1.2×10^{-4}; e.g. Meyer 1985; Feldman 1992). We have taken the Fe XVII ionic fraction as a function of temperature from the paper of Arnaud & Raymond (1992), which is similar to the more recent results of Mazzotta et al. (1998). Because of its stable Ne-like electron configuration, Fe XVII is the dominant ion over a broad temperature range, and its emission lines are among the brightest observed in astrophysical plasmas at temperatures around 3×10^6 K. The excitation rate for the 15.01 Å line ($2p^6 - 2p^5 3d\ ^1P_1$, Table 1) is taken from Smith et al. (1985), and it is very close to the results of other computations (e.g., Goldstein et al. 1989). The oscillator strength is from Bhatia & Doschek (1992). To obtain optical depths, we assume a line width of 30 km s^{-1}, typical of the solar corona (Mariska, Feldman & Doschek 1979). The emissivity and opacity for the range of temperatures we consider are displayed in Fig. 2.

2.3. Radiation Transfer

We perform the radiation transfer with a Monte Carlo radiation transfer code that accounts for arbitrary sources of emission and multiple scattering within an arbitrary geometry. The scattering code is based on that described by Code & Whitney (1995), but has now been modified to run on a three dimensional linear Cartesian grid (Wood & Reynolds 1999) and includes forced first scattering (Witt 1977) and a "peeling off"

procedure (Yusef-Zadeh, Morris, & White 1984). These modifications enable us to construct model images of three dimensional systems from specified viewing angles very efficiently.

For the current investigation we set up our grid with an RTV loop structure. The temperature dependent emissivity and opacity within the loop are determined as described above. We assume that all Fe XVII photons are emitted and resonantly scattered (with an isotropic scattering phase function) at a single wavelength. It is possible that when a 15.01 Å photon is absorbed, the excited level will decay to a 3p level, converting the energy into two EUV photons and a 3s-2p photon near 17 Å. However, the branching ratio for this conversion is only 5.7×10^{-4}, which can safely be ignored for the optical depths less than about 10 that we consider. We also assume that the photon does not leave the Doppler core. This is a good approximation for modest optical depths, though it would seriously underestimate the flux emerging in the line wings for large optical depths. We use the average scattering cross section over a Gaussian profile, rather than using the actual cross section as a function of velocity for computational speed.

3. Results

For each simulation of an RTV loop ($L = 10^{10}$cm) we form images at different viewing angles. In § 3.1 we show some representative Monte Carlo images that illustrate the effects of optical depth and viewing angle. From these images we compute the total emergent intensity for the particular viewing angle for comparison with an optically thin simulation (§ 3.2).

3.1. Images

In Figs. 3, 4, and 5 we show a set of model images for loops of different $T_{\max}$ at different viewing angles. We show optically thin images (assuming zero optical depth), and optically thick images with and without background plasma. In this and the following section we refer to viewing angles θ and ϕ, where the polar angle, θ, is measured from the z axis and the azimuthal angle, ϕ, is measured anti-clockwise from the x axis. In a Cartesian coordinate system, the loop is oriented in the $z - y$ plane (see Fig. 1). There are several features of the images that we now describe.

The $T_{\max}$ dependence affects the distribution of the emissivity along the loop. For the lowest temperature, $\log T_{\max} = 6.4$ (Fig. 3), the emissivity is concentrated towards the loop apex. This is because at $\log T_{\max} = 6.4$ the Fe XVII 15.01Å line emissivity is

almost zero (Fig. 2). This temperature occurs at the loop apex and the loop legs are cooler resulting in the concentration of emission at the apex and negligible emission from the loop legs. The emissivity distribution along the loop changes as we increase T_{max}. As T_{max} increases ($\log T_{\mathrm{max}} = 6.6$ in Fig. 4 and $\log T_{\mathrm{max}} = 6.8$ in Fig. 5) the emissivity becomes more concentrated towards the legs and footpoints of the loop. For $\log T_{\mathrm{max}} = 6.8$, the Fe XVII 15.01Å line emissivity is again almost zero (Fig. 2) and in this case the emission is concentrated towards the loop legs and there is negligible emission from the loop apex.

The geometrical line-of-sight effects for the optically thin images discussed by Alexander & Katsev are clearly seen in column A of Figs. 3, 4, and 5. When viewed from above, geometrical projection makes the footpoints appear bright (image A1 in Figs. 4 and 5), while the apex of the loop is brightened by projection if the loop is viewed edge-on (image A5 in Figs. 4 and 5). Loops that appear uniformly bright when seen face-on (image A3 in Figs. 3 and 4) appear to have bright looptops when viewed edge-on (image A5 Figs. 3 and 4). Similarly, loops that show brightening along the legs for face-on viewing (image A3 in Fig. 5), appear more uniformly illuminated when viewed edge-on (image A5 in Fig. 5). This is simply due to the increased path length towards the apex for edge-on loops.

Optical depth drastically reduces the geometrical projection effects because the long path length that enhances the brightness of an optically thin line implies a large optical depth for an optically thick line. The effect on image morphology is that isolated loops appear more uniformly bright (compare columns A and B in Figs. 3, 4, and 5). This arises because we see emission originating from the "optical depth one surface" which covers a progressively larger projected area on the loop as it becomes optically thicker. This effect is shown quantitatively in Fig. 6 where we show the intensity variation across two of the loop images from Fig. 4. Figure 6a shows the intensity variation across the images in Fig. 4 for the overhead view (images A1 and B1 in Fig. 4). The solid line shows the intensity variation across the optically thin image (image A1 in Fig. 4) with the intensity peak towards the legs of the loop evident. The dotted line shows the intensity variation for the same loop, but with the effects of resonant scattering included (image B1 in Fig. 4) — the overall intensity level is lower and the intensity variation is more uniform. Figure 6b shows the intensity variation across the images in Fig. 4 for the edge-on view (images A5 and B5 in Fig. 4). Again the solid line shows the intensity variation along the optically thin image (image A5 in Fig. 4) showing the intensity peak at the loop apex. The dotted line shows a much reduced intensity level and more uniform intensity for the loop model that includes resonant scattering effects (image B5 in Fig. 4).

Real solar active regions are complex structures, with loops of differing T_{max}, length and pressure. The emissivity scales as n_e^2, while the opacity scales as n_e, so that dense, low-lying

loops may dominate the emission, but a background plasma may provide additional Fe XVII scattering opacity. We simulate this effect by embedding the emitting loop in a lower density background (column C in Figs. 3, 4, and 5). The total emission from the background is half that from the RTV loop but the background is very diffuse (see Table 2), so the RTV loops are clearly visible.

Two main effects of the background opacity are easily seen in Fig. 5. The first is the scattered light halo present around the loops (e.g., image C5 in Fig. 5), arising from scattering of loop emission in the background plasma. Such halos might appear as fuzziness in EIT or TRACE images in EUV emission lines. The second effect is that the loop emission must pass through the background plasma and when the optical depth is large this results in scattering out of the line of sight and an asymmetry between the near and far side of the loops, resulting in an apparent one-sided loop (e.g., image C4 in Fig. 5). Asymmetric loops are often observed in SOHO/EIT and TRACE images (examples may be seen on the TRACE homepage: http://vestige.lmsal.com/TRACE/Public/Gallery/Images/). Most are probably asymmetric in reality, but optical depth may play a role in some observed morphologies.

We note that the 171 and 195 Å bands of EIT and TRACE and the 284 Å band of EIT are dominated by resonance lines of Fe IX, Fe X, Fe XII and Fe XV. While these ions do not occupy as large a temperature range as Fe XVII, the scattering cross section scales in proportion to wavelength, and images in these lines are likely to show similar effects to those predicted for Fe XVII (it is the line optical depth and not the wavelength that determines the image morphology in our simulations). Indeed, Schrijver & McMullen (2000) have inferred that scattering effects are important from the variation of intensity with height above the limb from TRACE and EIT images.

3.2. Unresolved Intensity

In the previous section we showed spatially resolved model images in the light of the Fe XVII line, as may be observed in the solar corona. Observations of stellar coronae cannot spatially resolve coronal loops and the CHANDRA satellite has recently observed Capella and other active late-type stars as part of the Emission Line Project. As our resolved images showed, optically thick resonant scattering yields image morphologies and intensity distributions along the loops that differ from optically thin simulations. In this section we investigate the effects of optically thick resonant scattering on the Fe XVII line intensity for different orientations of unresolved loops, and compare it with the intensity expected if the line were optically thin. For optically thin emission all emitted photons escape from the

source isotropically, and all loops will yield the same intensity independent of viewing angle. Optical depth effects result in photons exiting the simulation region preferentially along optically thinner sightlines. Also, for optically thick loops, the intensity is proportional to the projected area of the loop, so face-on loops will yield larger intensities than edge-on loops.

Figure 7 shows the intensity ratio for an unresolved optically thick model compared to the corresponding model when optical depth effects are ignored. Each panel shows the intensity ratio for a range of T_{max}, with the individual curves showing different viewing angles of the loop.

The left column shows intensity ratios for an isolated RTV loop (no background plasma). Face-on viewing ($\phi = 0$, $\theta = \pi/2$) results in intensities that are larger than the optically thin case, due to photons being scattered into our line of sight. For edge-on viewing ($\phi = \pi/2$, $\theta = \pi/2$), the intensity is lower than the optically thin case. This is for two reasons; firstly the projected emitting area is smaller for edge-on loops (see the loop images in Figs. 3, 4, and 5). Secondly as the optical depth increases, photons from the far side of the loop have to traverse a greater optical depth through the loop and are more likely to be scattered into the optically thinner face-on directions. Depending on T_{max} and loop orientation, the intensity can range from being 20% brighter to 50% fainter than the intensity from an optically thin loop.

The second column in Fig. 7 shows intensity ratios for loops embedded within a background plasma. The background has a temperature of $T_{\mathrm{back}} = 2.5 \times 10^6 \mathrm{K}$ and the density is chosen so that the total intensity from the background is half that from the loop (Table 2). The optically thick to optically thin intensity ratios for these simulations show that the intensity ranges from around 60% to 120% of the optically thin intensity depending on T_{max} and viewing angle. These simulations show that optical depth, geometry, and loop orientation can have a large effect on observed line ratios. Clearly great care is required in interpreting coronal images and line ratios due to the effects of projection and optically thick resonant scattering.

4. Summary

Our simulations have shown that optical depth effects, both within loops and in a background plasma, can change the amount of intensity emerging into a given direction and also the image morphology. Intensity ratios may vary in the range 50% to more than 120% of their optically thin values. If one observes an ensemble of loops, for instance

spread over the surface of another star, the effects tend to average out. Equal numbers of photons are scattered into and out of the line of sight. However, a net effect may still arise if the emissivity and opacity vary in different ways. Given the electron density factor in the emissivity and its absence in the opacity, such differences are likely. To account for the general trend of reduced Fe XVII 15.01 Å intensity (e.g. Saba et al. 1999) by scattering rather than errors in atomic rates, the typical structure must preferentially scatter photons down to the solar surface. Such an example may be emission from dense, low-lying loops that is scattered in a more diffuse, larger scale region. This is expected from RTV models and is observed in solar active regions. Models similar to those in the righthand column of Fig. 5 can easily be constructed to reduce the intensities of lines having large oscillator strengths. They may be invoked when line ratio anomalies appear in Chandra or XMM data. Proving that optical depth is indeed the explanation for a given anomaly will undoubtably be a challenge.

REFERENCES

Alexander, D., & Katsev, S. 1996, Sol. Phys. 167, 153

Arnaud, M.A., & Raymond, J.C. 1992, ApJ, 398, 394

Bhatia, A.K., & Kastner, S.O. 1999, ApJ, 516, 482

Bhatia, A.K., & Doschek, G.A. 1992, ADNDT, 52, 1

Brown, G.V., Beiersdorfer, P., Leidahl, D.A., Widmann, K., & Kahn, S.M. 1998, ApJ, 502, 1015

Code, A.D., & Whitney, B.A. 1995, ApJ, 441, 400

Feldman, U. 1992, Physica Scripta, 46, 202

Goldstein, W.H., Osterheld, A., Oreg, J., & Bar-Shalom, A. 1989, ApJ, 344, L37

Kastner, S.O., & Kastner, R.E. 1990, JQSRT, 44, 275

Mariska, J.T., Feldman, U., & Doschek, G.A. 1979, A&A, 73, 361

Mazzotta, P., Mazzitelli, G., Colafrancesco, S., & Vittorio, N. 1998, A&AS, 133, 403

Meyer, J.P., 1985, ApJS, 57, 173

Rosner, R., Tucker, W.H., & Vaiana, G.S. 1978, ApJ, 220, 643

Phillips, K.J.H., Greer, C.J., Bhatia, A.K., Coffey, I.H., Barnsley, R., & Keenan, F.P. 1997, A&A, 324, 381

Rugge, H.R., & McKenzie, D.L. 1985, ApJ, 297, 338

Saba, J.L.R., Schmelz, J.T., Bhatia, A.K., & Strong, K.T. 1999, ApJ, 510, 1064

Schmelz, J.T., Saba, J.L.R., Chauvin, J.C., & Strong, K.T. 1997, ApJ, 477, 509

Schrijver, C.J., & McMullen, R.A. 2000, ApJ, in press

Smith, B.W., Mann, J.B., Cowan, R.D., & Raymond, J.C.1985, ApJ, 298, 898

Waljeski, K. et al. 1994, ApJ, 429, 909

Witt, A.N., 1977, ApJS, 35, 1

Wood, K., & Reynolds, R.J. 1999, ApJ, 525, 799

Yusef-Zadeh, F., Morris, M., & White, R.L. 1984, ApJ, 278, 186

Table 1.   Oscillator Strengths for Various Fe XVII Lines

λ (Å)	Transition	f
15.01	$2p^6 - 2p^5 3d\ ^1P_1$	2.66
15.25	$2p^6 - 2p^5 3d\ ^3D_1$	0.59
15.46	$2p^6 - 2p^5 3d\ ^3P_1$	0.0089
16.79	$2p^6 - 2p^5 3s\ ^1P_1$	0.10
17.05	$2p^6 - 2p^5 3s\ ^3P_1$	0.12
17.10	$2p^6 - 2p^5 3s\ ^3P_2$	0.00

Table 2.   RTV Loop T_{max}, Background Temperature and Density

$\log T_{\mathrm{max}}$	$\log T_{\mathrm{back}}$	n_{back} (cm^{-3})
6.4	6.4	0.24×10^8
6.5	6.4	0.70×10^8
6.6	6.4	1.60×10^8
6.7	6.4	3.00×10^8
6.8	6.4	6.00×10^8
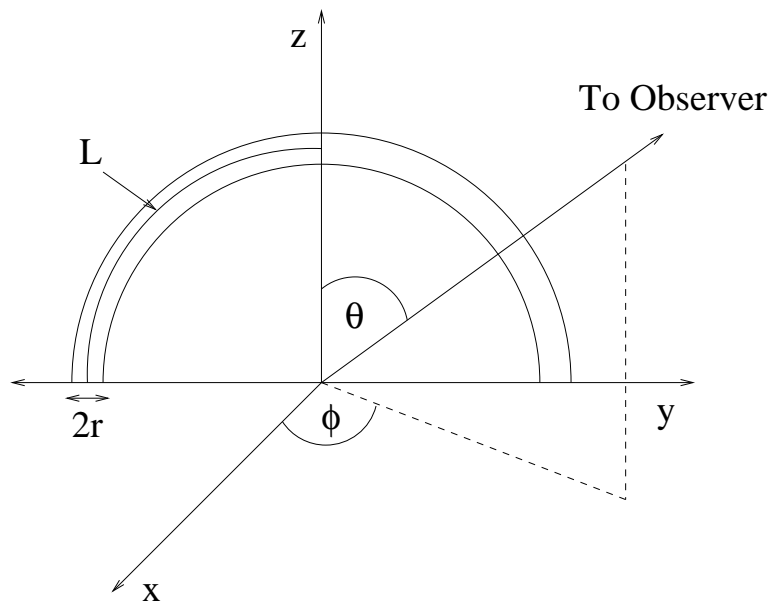
Fig. 1.— Diagram showing the length, L, radius, r, and orientation (θ, ϕ) of an RTV loop in our simulations.
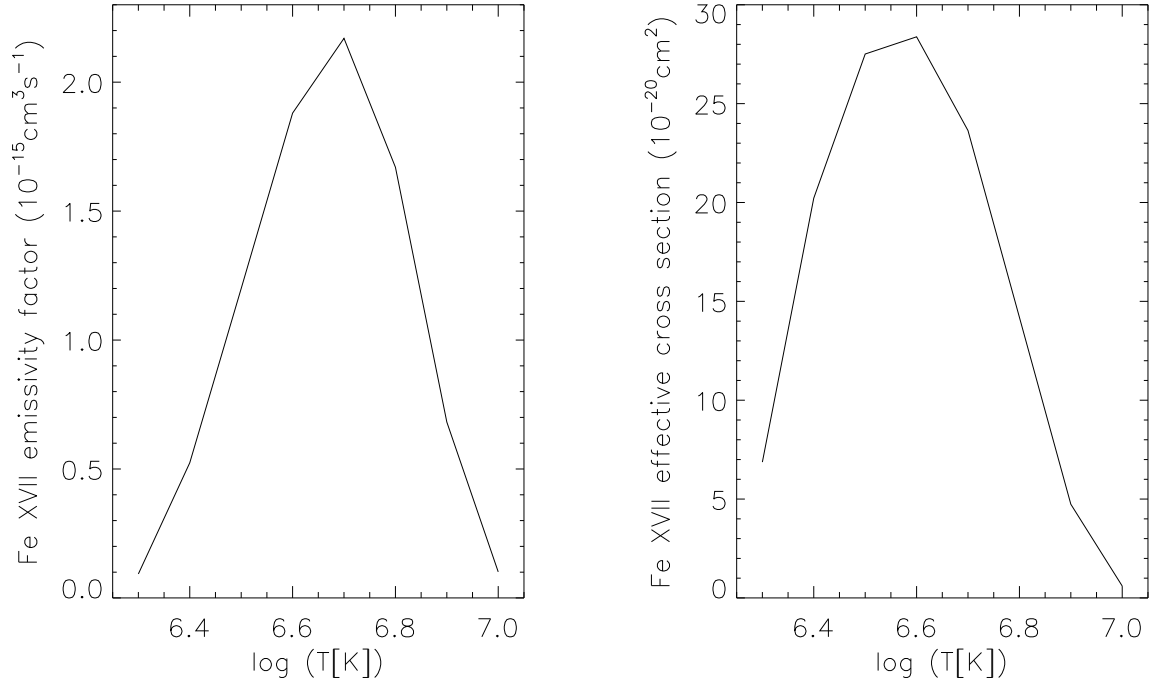
Fig. 2.— Emissivity and effective scattering cross section for the Fe XVII 15.01Å line as a function of temperature. The effective cross section includes the Fe abundance and Fe XVII fractional concentration.
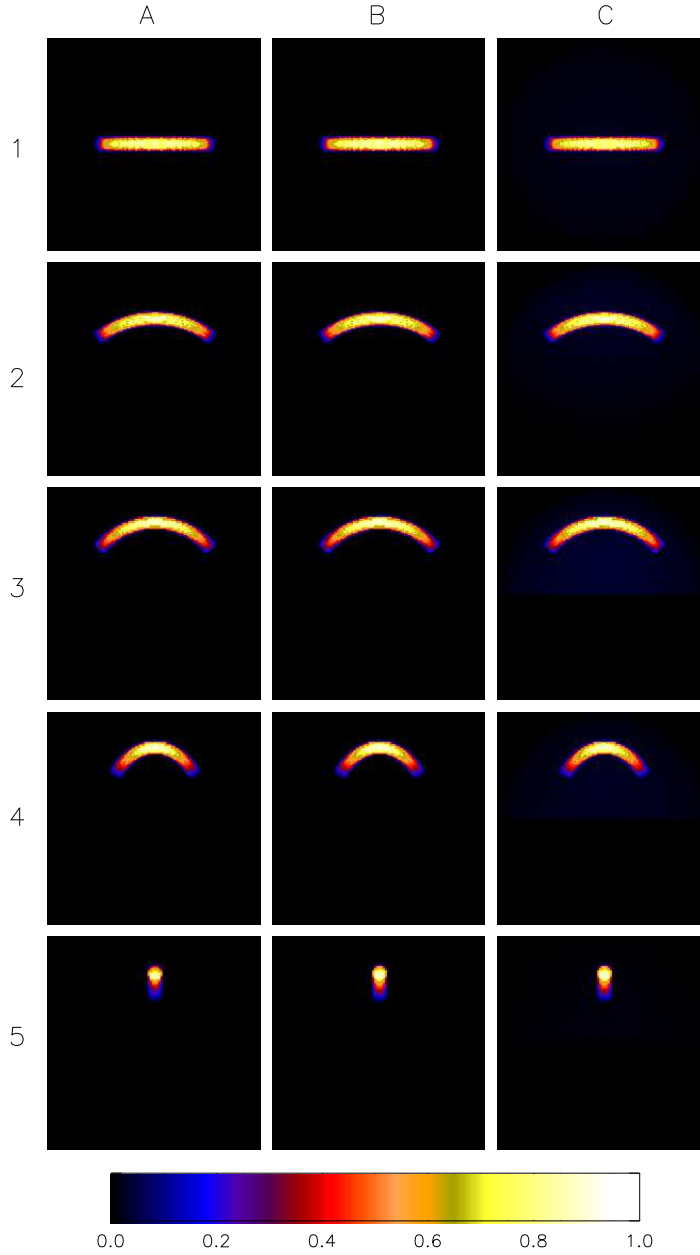
Fig. 3.— Loop images at different viewing angles for $\log T_{\max} = 6.4$, where $T_{\max}$ is the maximum temperature of the RTV loop. Each column shows appearance of a loop as viewed from (top to bottom) directly above (1), 45° from vertical (2), face-on (3), rotated by 45° (4), and edge-on (5). Column A shows optically thin images, column B is an optically thick isolated loop, column C is a loop embedded in a background plasma ($T = 2.5 \times 10^6$K, $n_e = 2.4 \times 10^7$cm^{-3}). Each image is 3×10^{10}cm on a side.
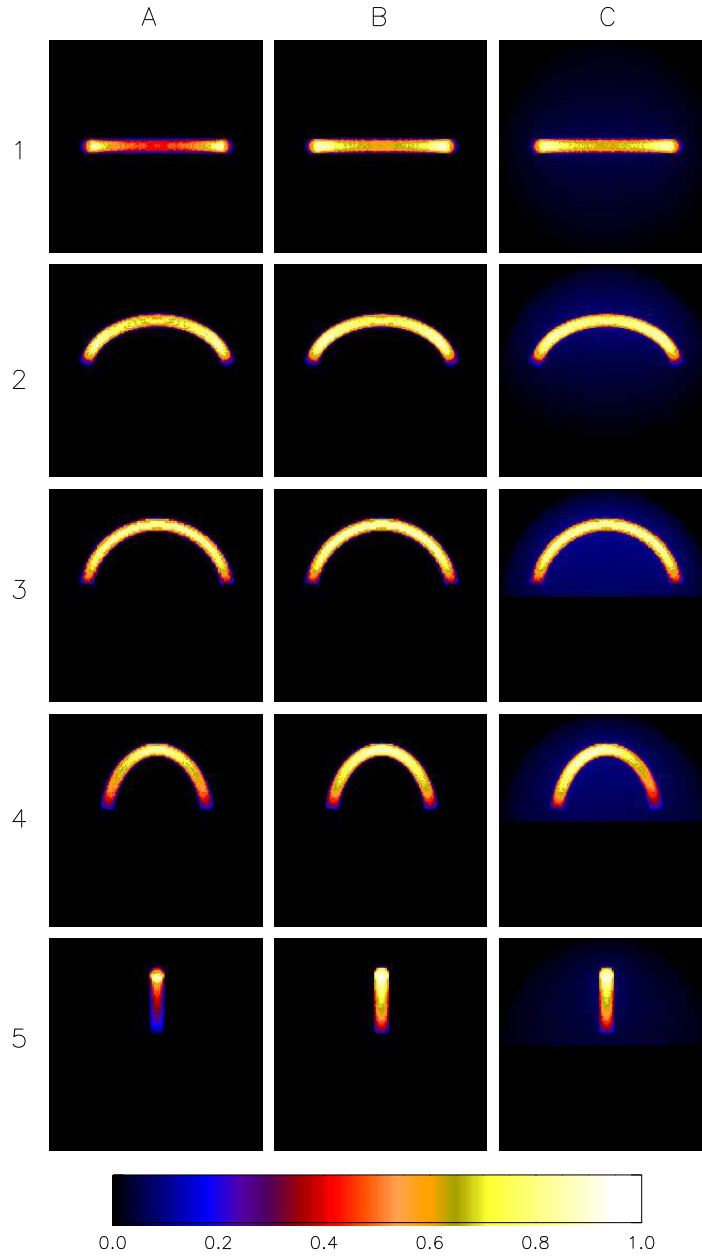
Fig. 4.— As Fig. 3, but $\log T_{\mathrm{max}} = 6.6$ and a background plasma for column C of $T = 2.5 \times 10^6 \mathrm{K}$, $n_e = 1.6 \times 10^8 \mathrm{cm}^{-3}$.
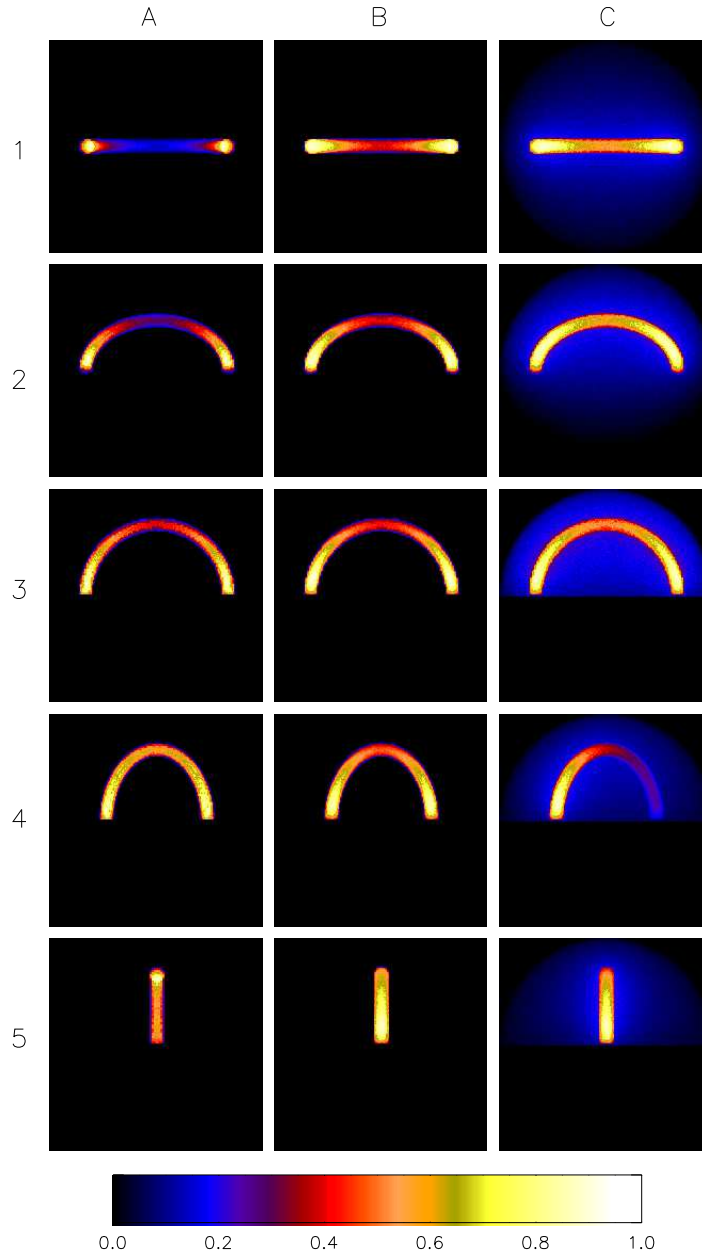
Fig. 5.— As Fig. 3, but $\log T_{\max} = 6.8$ and a background plasma for column C of $T = 2.5 \times 10^6 \mathrm{K}$, $n_e = 6 \times 10^8 \mathrm{cm}^{-3}$.
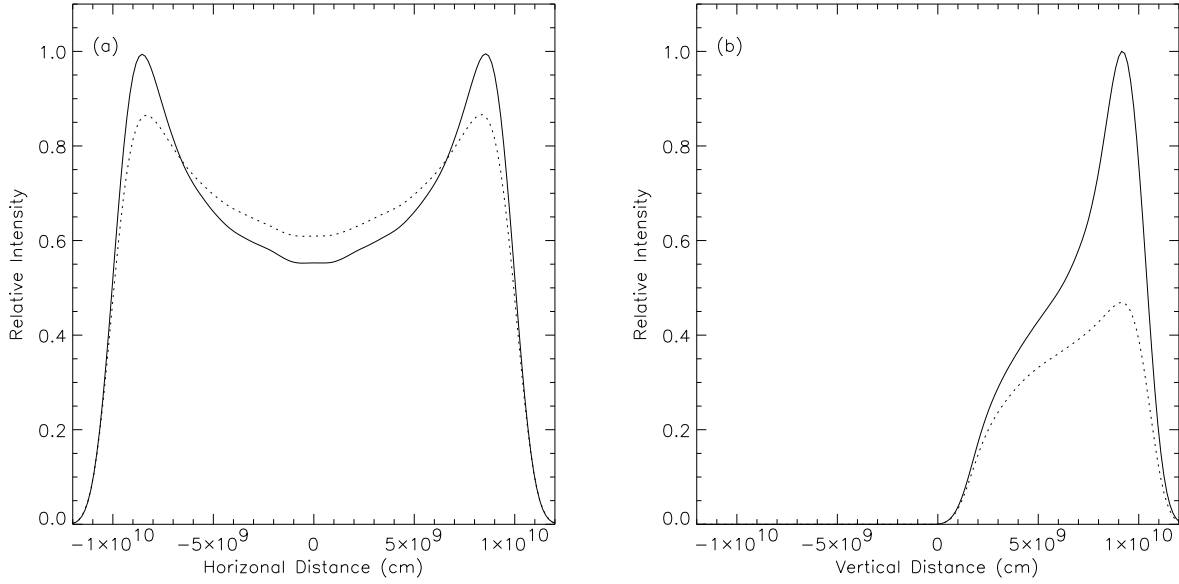
Fig. 6.— (a) Solid line: intensity variation across image A1 in Fig. 4 (loop viewed from above) showing the intensity peak towards the loop legs for this optically thin simulation. Dotted line shows intensity variation for the same loop model, but including resonant scattering effects (image B1 in Fig. 4). (b) As for (a), but for images A5 and B5 in Fig. 4 (loop viewed edge-on).
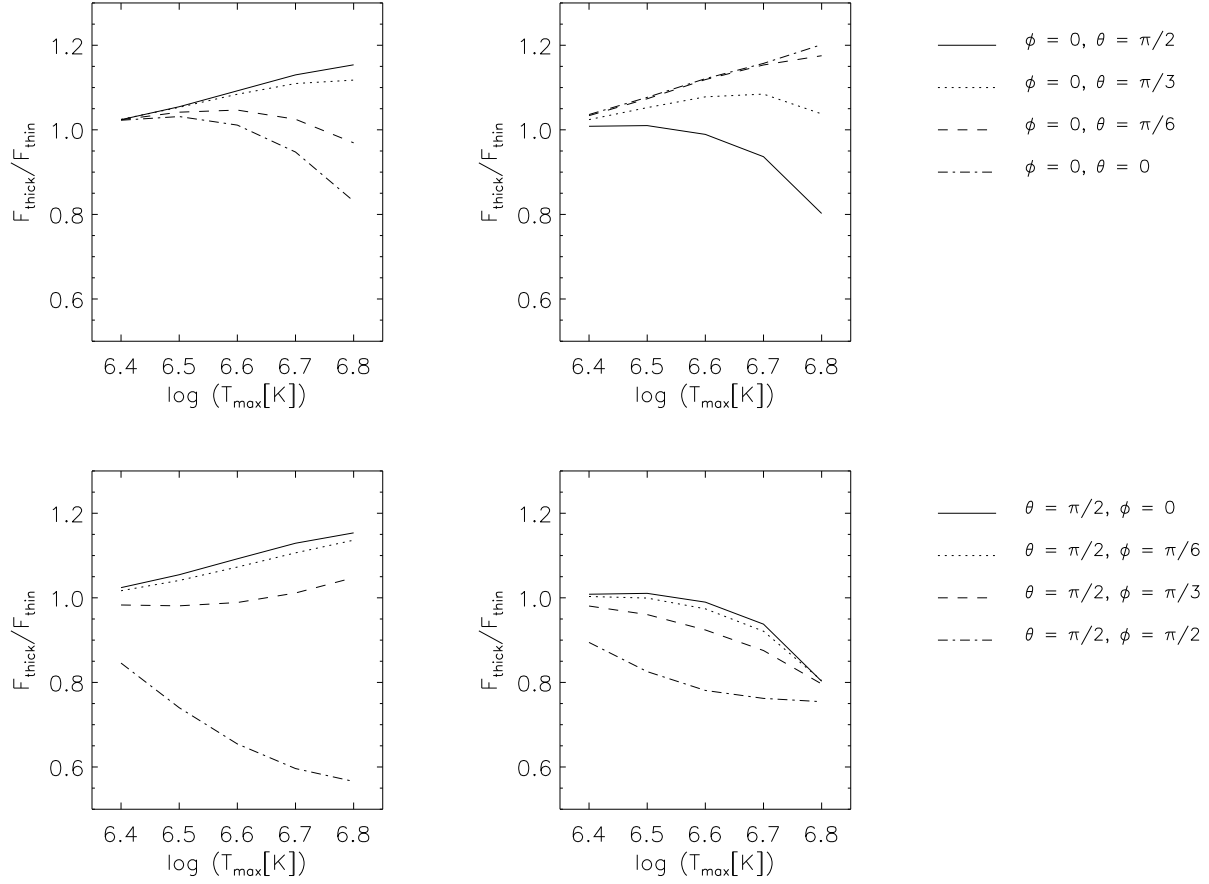
Fig. 7.— Optically thick to optically thin intensity ratios as a function of maximum loop temperature. Each panel shows the intensity ratios for different loop viewing angles. Left most column shows ratios for isolated loops, second column for a loop embedded in a background plasma. Line types are for different viewing angles, upper row rotating through θ, lower row rotating through ϕ.